

ORIGINAL RESEARCH ARTICLE

Plasmalogen enrichment in exosomes secreted by a nematode parasite versus those derived from its mouse host: implications for exosome stability and biology

Fabio Simbari¹, Jana McCaskill¹, Gillian Coakley¹, Marissa Millar¹,
Rick M. Maizels^{1,2}, Gemma Fabriás³, Josefina Casas³ and Amy H. Buck^{1*}

¹Institute of Immunology and Infection Research and Centre for Immunity, Infection and Evolution, School of Biological Sciences, University of Edinburgh, Edinburgh, UK; ²Wellcome Trust Centre for Molecular Parasitology, Institute of Infection, Immunology and Inflammation, University of Glasgow, Glasgow, UK; ³Department of Biomedical Chemistry, Institute of Advanced Chemistry of Catalonia, Spanish Council for Scientific Research (IQAC-CSIC), Barcelona, Spain

Extracellular vesicles (EVs) mediate communication between cells and organisms across all 3 kingdoms of life. Several reports have demonstrated that EVs can transfer molecules between phylogenetically diverse species and can be used by parasites to alter the properties of the host environment. Whilst the concept of vesicle secretion and uptake is broad reaching, the molecular composition of these complexes is expected to be diverse based on the physiology and environmental niche of different organisms. Exosomes are one class of EVs originally defined based on their endocytic origin, as these derive from multivesicular bodies that then fuse with the plasma membrane releasing them into the extracellular environment. The term exosome has also been used to describe any small EVs recovered by high-speed ultracentrifugation, irrespective of origin since this is not always well characterized. Here, we use comparative global lipidomic analysis to examine the composition of EVs, which we term exosomes, that are secreted by the gastrointestinal nematode, *Heligmosomoides polygyrus*, in relation to exosomes secreted by cells of its murine host. Ultra-performance liquid chromatography – tandem mass spectrometry (UPLC-MS/MS) analysis reveals a 9- to 62-fold enrichment of plasmalogens, as well as other classes of ether glycerophospholipids, along with a relative lack of cholesterol and sphingomyelin (SM) in the nematode exosomes compared with those secreted by murine cells. Biophysical analyses of the membrane dynamics of these exosomes demonstrate increased rigidity in those from the nematode, and parallel studies with synthetic vesicles support a role of plasmalogens in stabilizing the membrane structure. These results suggest that nematodes can maintain exosome membrane structure and integrity through increased plasmalogens, compensating for diminished levels of other lipids, including cholesterol and SM. This work also illuminates the prevalence of plasmalogens in some EVs, which has not been widely reported and could have implications for the biochemical or immunomodulatory properties of EVs. Further comparative analyses such as those described here will shed light on diversity in the molecular properties of EVs that enable them to function in cross-species communication.

Keywords: *extracellular vesicles; helminth; host–pathogen; ether lipids; dynamic light scattering; cholesterol; cross-species communication*

Responsible Editor: Andrew Hill, La Trobe University, Australia.

*Correspondence to: Amy H. Buck, Ashworth Laboratories, King's Buildings, Charlotte Auerbach Road, Edinburgh EH9 3FL, UK, Email: a.buck@ed.ac.uk

To access the supplementary material to this article, please see [Supplementary files](#) under 'Article Tools'.

Received: 16 December 2015; Revised: 31 May 2016; Accepted: 6 June 2016; Published: 5 July 2016

Extracellular vesicles (EVs) are secreted by virtually all organisms and cell types and are involved in intercellular communication processes (1). One class of EVs, exosomes, originate from the late endosomal

compartment due to inward budding of the multivesicular bodies (MVBs). MVBs that escape lysosomal degradation can fuse with the plasma membrane and release their contents including vesicles into the extracellular

environment (2,3). Practically, however, this term is often used to describe any small EVs recovered by high-speed ultracentrifugation, since the intracellular origin of the vesicles is not always well characterized. Exosomes were first described in the 1980s in the context of reticulocyte maturation (4–6) and later characterized by Raposo et al. (7) as antigen-presenting vesicles in B lymphocytes. Over the last few decades, exosomes and other classes of EVs have received a renewed interest by the scientific community based on their implications in numerous disease contexts including cancer and infection (8). EVs have also been found to be produced by diverse parasites and can alter the properties of immune cells (9,10). Indeed, the secretion and subsequent uptake of EVs has also been proposed as a mechanism of communication between organisms and between different species. For example, exosome-like nanoparticles have been isolated from edible plants and fruits, and their beneficial anti-inflammatory and antioxidative effects have been suggested in a mouse model (11–13). The extent to which EVs operate between phylogenetically distinct species is not yet clear, but this could provide a broad-reaching mechanism for communication and exchange of genetic information. However, little is known about the comparative properties of EVs from diverse sources and the features that make them functional in a specific environment.

We recently reported that the gastrointestinal nematode parasite *Heligmosomoides polygyrus* secretes small EVs recovered by high-speed centrifugation, which we have called exosomes, that can be internalized by mouse intestinal epithelial cells and can transfer parasite material, including microRNAs, to host cells (14). It is intriguing to think that the nematode has evolved exosomes as an immunomodulatory complex that is particularly well-suited to the mouse intestinal environment. Lipids are a key component of exosomes as their lipid bilayer is directly exposed to the environment and represents the interacting surface with recipient cells. Remarkably, the lipid content of EVs across different species still remains relatively unexplored: a small fraction of the total entries for vesicle cargo collected in the online database Vesiclepedia are devoted to lipids (15). Of the limited lipidomic studies published, these mainly describe the lipid composition of human-derived exosomes or other EVs from mast cells, B cells, DC, reticulocytes, cancer cell lines and semen (16–20), reviewed in (21).

In mammalian systems, cholesterol and sphingomyelin (SM) are key to membrane fluidity and stability (22), and accordingly, exosomes from multiple sources have been described as highly enriched in these lipids compared with producing cells (23). It is unknown whether cholesterol and SM would play similar roles in nematode-derived exosomes, whose lipid content has not been previously examined. Nematodes are not believed to synthesize cholesterol or other sterols *de novo* but largely derive them from their diet (24,25). Furthermore, although SM

has been reported in helminths, the biogenesis pathways are not well characterized and may be variable across species (26). Here, we performed a biochemical characterization of the exosomes secreted by *H. polygyrus* in comparison to murine exosomes derived from 2 cell types present in proximity to the parasite in the gut environment: small intestinal epithelial cells and macrophages. The aim was to thoroughly investigate the lipid composition of each type of exosome in order to underpin their potential implications in exosome stability or functional capacity.

Methods

Exosome purification from HES products

For collection of HES products, CF1 mice were infected with infective-stage larvae (L3) by gavage and adult parasites harvested from the small intestine 14 days postinfection. The worms were maintained in serum-free media *in vitro* as previously described (14,27). Prior to concentration of HES, eggs were removed by centrifugation at 400g and media were filtered through a 0.2- μ m filter (Millipore). Vesicles were consequently isolated from filtered medium following a modified version of the standard protocol used for exosomes isolation (28). Media were first centrifuged at 100,000g for 90 min using polyallomer tubes (Beckman Coulter) at 4°C in a SW40 rotor (Beckman Coulter). Pelleted material was washed twice in filtered PBS at 100,000g for an additional 90 min. The supernatant was concentrated using Vivaspin 6500 K MWCO tubes (Fisher) at 5,000g and washed twice in PBS.

Mammalian cells culture and exosomes isolation

MODE-K were obtained from Dominique Kaiserlian (INSERM) (29) and Raw 264.7 cells from ATCC and were screened on a monthly basis for mycoplasma contamination. These were cultured, respectively, in DMEM and RPMI media (Invitrogen), supplemented with 10% foetal bovine serum (Invitrogen), 1% penicillin–streptomycin (Lonza) and 1% L-glutamine (Lonza). An additional 1% of non-essential amino acids (NEAA)/sodium pyruvate (NaPy; Gibco) was used to complement MODE-K cell medium. Prior to exosome isolation, MODE-K cells were shifted to serum-free advanced DMEM medium (Invitrogen) supplemented with 1% L-glutamine (Lonza), whereas Raw 264.7 were cultured in complete medium containing 10% of FBS previously depleted of exosomes (100,000g overnight at 4°C). For exosome isolation, cells were first cultured in T-150 cm² flasks including 10% FBS. When they reached ~30% confluency, the media was aspirated, cells were washed twice and shifted to the media depleted of FBS or the exosome-depleted FBS as described above. After 48-h incubation, the media was collected and centrifuged at 2,000g for 30 min to remove cell debris. Supernatants were further filtered through 0.22- μ m Millex GP filter units

(Millipore) and ultra-centrifuged (100,000g, 90 min at 4°C) in Polyallomer Centrifuge Tubes (Beckman Coulter). Pelleted material was washed twice in filtered PBS at 100,000g for an additional 90 min. After the second wash, pellets were resuspended in ~200 µl PBS. The total protein content of exosomes was determined using a Qubit 2.0 Fluorometer according to the manufacturer's protocol.

Transmission electron microscopy

For visualization of the vesicles, the purified ultracentrifuge pellets from *H. polygyrus* HES and murine cell culture conditioned media (100 µg/ml protein concentration) were fixed in 2% PFA, deposited on Formvar-carbon coated TEM grids and treated with glutaraldehyde prior to treatment with uranyl oxalate and methyl cellulose as described in (28). Images were taken on a Gatan Orius CCD camera.

Western blot analysis of exosomes

Primary antibodies were purchased from Cell Signaling (ALIX clone 3A9, β-actin) and Abcam (CD9). The overall protein content of nematode and mouse exosomes was measured based on the BCA protein assay kit (Life Technologies) according to the manufacturer's instructions. Equal amounts (3 µg) of protein from the exosomal or cell lysates were loaded onto 4–12% NuPage Bis-Tris polyacrylamide gel and subjected to sodium dodecyl-polyacrylamide gel electrophoresis (SDS–PAGE). After transfer, nitrocellulose membranes were blocked with 5% non-fat dried milk in PBS, 0.1% Tween 20 (PBS-T) and incubated overnight at 4°C with primary antibodies in 5% milk, PBS-T. Membranes were washed with PBS-T (3 × for 10 min) before incubation with the appropriate HRP-conjugated secondary antibodies (1:5,000) in 5% milk/PBS-T. After washing (for 10 min in PBS-T, 3 ×), enhanced chemiluminescence was used to visualize bands.

Silver staining

Samples (2 µg of protein) were subjected to SDS–PAGE as described above. After electrophoresis, gels were left (2–3 h) in fixer solution (10% acetic acid and 40% ethanol) followed by sensitization (30 min) using 0.02% sodium thiosulfate/sodium acetate solution. After washing with deionised water (3 ×, 5 min), gels were incubated in silver nitrate (0.5%, w/v, water solution) for 20 min and protected from light. Gels were then washed in water (1 min, 2 ×) and developed (2–15 min) using a 3% sodium carbonate solution, 0.02% PFA (stock at 37%). The reaction was stopped using EDTA-Na₂ at 10 mM. Gel images were acquired using HP Photosmart C4280 scanner.

DLS studies

Exosome size, PDI and zeta-potential were obtained using the Zetasizer Nano ZS90 (Malvern Instruments, Worces-

tershire, UK). For size measurements, exosomes (5 µg) were suspended in PBS, whereas a solution of exosomes/PBS:H₂O (1:10) was used to measure the Z-potential of the vesicles. Samples were analysed at constant temperature (25°C) and data were acquired and analysed using the proprietary Malvern software.

LC–MS analysis

PLs and SLs extracts were prepared and analysed using the following protocols (30,31), with minor modifications. A total of 60 µg of exosomes (total protein amount) in 0.1 ml PBS was transferred to borosilicate glass test tubes with Teflon caps, and 0.25 ml methanol and 0.5 ml chloroform were subsequently added. This mixture was fortified with internal standards of lipids (200 pmol each). The following di-acyl PLs standards were used: 16:0 D31–18:1 phosphocholine, 16:0 D31–18:1 phosphoethanolamine and 16:0 D31–18:1 phosphoserine. Each standard presents a deuterated C16:0 acyl chain in the sn-1 position of the glycerol. As for the lyso-PLs, standards with a non-natural odd carbon chain (C 17:1) were chosen for each phosphocholine, phosphoethanolamine and phosphoserine polar head. As internal SL standards, *N*-dodecanoylsphingosine and *N*-dodecanoylsphingosyl phosphorylcholine were used for Cers and SMs, respectively, and *N*-dodecanoylglucosylsphingosine was the standard for glucosyl/galactosyl ceramides and lactosyl ceramides. Samples were vortexed and sonicated until they appeared dispersed and incubated overnight at 48°C. The samples were then evaporated and transferred to 1.5 ml eppendorf tubes after the addition of 0.5 ml of methanol. Samples were evaporated again and resuspended in 150 µl of methanol. The tubes were centrifuged at 10,000 rpm for 3 min, and 130 µl of the supernatants was transferred to ultra-performance liquid chromatography (UPLC) vials for injection and analysis of PLs. After injection, samples were recovered and incubated with 75 µl of 1 M KOH in methanol for 2 h at 37°C, and KOH was neutralized with 75 µl of 1 M acetic acid. The samples were then evaporated and transferred to 1.5 ml eppendorf tubes after the addition of 0.5 ml of methanol. Samples were evaporated again and resuspended in 150 µl of methanol. The tubes were centrifuged at 10,000 rpm for 3 min, and 130 µl of the supernatants was transferred to UPLC vials for injection and analysis of SLs.

The LC–MS analysis consisted of a Waters Acquity UPLC system connected to a Waters LCT Premier orthogonal accelerated time-of-flight mass spectrometer (Waters), operated in both positive and negative electrospray ionization (ESI) mode. Full-scan spectra from 50 to 1,500 Da were acquired, and individual spectra were summed to produce data points each of 0.2 s. Mass accuracy and reproducibility were maintained by using an independent reference spray (leucine enkephalin) via

the LockSpray interference. The analytical column was a 100 × 2.1 mm inner diameter and 1.7-mm C8 Acquity UPLC-bridged ethylene hybrid (Waters). The 2 mobile phases were methanol (phase A) and water (phase B), both contained 0.2% formic acid (v/v) and 2 mM ammonium formate. A linear gradient was programmed as follows – 0.0 min: 20% B; 3 min: 10% B; 6 min: 10% B; 15 min: 1% B; 18 min: 1% B; 20 min: 20% B; 22 min: 20% B. The flow rate was 0.3 ml/min. The column was held at 30°C.

Positive identification of compounds was based on the accurate mass measurement with an error < 5 ppm and its LC retention time, compared with that of a standard ($\pm 2\%$). SLs and lipids with phosphocholine polar heads were analysed in positive ESI mode, whereas lipids with phosphoethanolamine and phosphoserine polar heads were analysed in negative ESI mode. Cer standards used were *N*-palmitoyl-sphingosine, *N*-stearoyl-sphingosine, *N*-lignoceroyl-sphingosine and *N*-nervonoyl-sphingosine. DHcer standards used were *N*-palmitoyl-dihydro-sphingosine, *N*-stearoyl-dihydro-sphingosine, *N*-lignoceroyl-dihydro-sphingosine and *N*-nervonoyl-dihydro-sphingosine. SM standards used were *N*-palmitoylsphingosyl phosphorylcholine, egg SMs (predominant C16:0SM) and brain SMs (C18:0SM, C24:0SM and C24:1SM in known percentages). Glucosylceramide standard used was *N*-palmitoylglucosylsphingosine. Lactosylceramide standard used was *N*-palmitoyl-lactosylsphingosine. Diacylphospholipid standards used were 1,2-dipalmitoyl-*sn*-glycero-3-phosphocholine, 1-palmitoyl-2-oleoyl-*sn*-glycero-3-phosphocholine, 1-palmitoyl-2-oleoyl-*sn*-glycero-3-phosphoethanolamine and 1-palmitoyl-2-oleoyl-*sn*-glycero-3-phospho-L-serine. Lysophospholipid standards used were 1-stearoyl-2-hydroxy-*sn*-glycero-3-phosphocholine, 1-oleoyl-2-hydroxy-*sn*-glycero-3-phosphoethanolamine and 1-oleoyl-2-hydroxy-*sn*-glycero-3-phospho-L-serine. Ether-lipid standards used were (plasmalogen)-C18:1 phosphocholine (1-(1Z-octadecenyl)-2-oleoyl-*sn*-glycero-3-phosphocholine), C18 (plasmalogen)-C18:1 phosphoethanolamine (1-(1Z-octadecenyl)-2-oleoyl-*sn*-glycero-3-phosphoethanolamine), C18 (plasmalogen) lyso phosphocholine (1-*O*-1'-(Z)-octadecenyl-2-hydroxy-*sn*-glycero-3-phosphocholine) and C18 (plasmalogen) lyso phosphoethanolamine (1-*O*-1'-(Z)-octadecenyl-2-hydroxy-*sn*-glycero-3-phosphoethanolamine). When authentic standards were not available, identification was achieved based on their accurate mass measurement, elemental composition, calculated mass, error, double-bond equivalents and retention times.

Quantification was carried out using the extracted ion chromatogram of each compound, using 50 mDa windows. The linear dynamic range was determined by injecting mixtures of internal and natural standards as indicated above. Since standards for all identified lipids were not available, the amounts of lipids are given as pmol equivalents relative to each specific standard.

Cholesterol assay

Cholesterol levels were measured in exosomes (3 µg protein content) using the Amplex Red cholesterol assay kit that detects cholesterol and cholesteryl esters (Life Technologies) according to the manufacturer instructions.

Laurdan GP studies of membrane fluidity

Nematode and mouse exosomes (20 µg protein content) were labelled with Laurdan dye (0.2 µM final concentration) as described in (32). Incubations (45 min at 37°C, in the dark) were performed in 2.5 ml total volume of MES buffer (10 mM MES, 145 mM NaCl, 5 mM KCl, pH 6.0). After the incorporation of the dye, Laurdan GP excitation spectra (320–420 nm at both 435 and 490 nm emission wavelengths) were obtained at physiological temperature as previously described (33). Spectra were acquired using a computer-driven L-type spectrofluorometer (Fluoromax-3, Spex) equipped with a stirring accessory and thermostatted by a circulating water bath. The GP index was calculated according to the equation: $GP = (I_{440} - I_{490}) / (I_{440} + I_{490})$, where I_{440} and I_{490} are the emission intensities at each excitation wavelength (320–420 nm). GP values were calculated after subtraction of MES buffer fluorescence background signal.

Membrane fusion assay

The octadecyl rhodamine B chloride (R18) self-quenching lipophilic dye (Life Technologies) was used to measure the vesicles fusion efficiencies. Fusion activity was addressed as a direct reflection of the de-quenching and consequent increasing in fluorescence that takes place after the dye is diluted. Exosomes (20 µg protein content) or artificial vesicles (1 µM) were labelled using R18 (1 mM) in 500 µl of MES buffer (10 mM MES, 145 mM NaCl, 5 mM KCl, pH 6.0) during 30 min at room temperature. The unincorporated R18 was removed by using Exosomes Spin Columns 3,000 MW (Life Technologies) according to the manufacturer's protocol. Labelled vesicles were added to MES fusion buffer (final volume 2.5 ml), and fluorescence was monitored using a thermostatted spectrofluorometer FluoroMax-3 (Spex). Fluorescence was measured continuously at 560-nm excitation and 590-nm emission wavelengths (slits 1.5 nm) as previously described in (33). The fluorescence of the labelled vesicles was examined over a 30-min period prior to addition of unlabelled MODE-K cells (1×10^6) were added to the exosomes, and fluorescence was monitored for a further 30 min. Following an additional 30-min incubation, the fusion reaction was stopped by the addition of Triton X-100 (0.3% final concentration), which resulted in maximal probe dilution. The fluorescence increase was measured as the difference with respect to the initial fluorescence of labelled exosomes and expressed as % of maximal FD according to the equation, $\% FD = ((F - F_i) / (F_{max} - F_i)) \times 100$, where F is the fluorescence intensity after 30 min of incubation of exosomes + cells, F_i is the initial fluorescence

of labelled exosomes and F_{\max} is the fluorescence intensity after detergent membrane disruption. Background fluorescence values obtained for each condition but in the absence of the labelled vesicles (MES buffer, MES + cells, MES + cells + Triton X-100) were subtracted from the registered F , F_i and F_{\max} values, respectively.

Artificial vesicles formulation

Artificial vesicles were custom made by Excytex BV (Utrecht, The Netherlands). The acyl phospholipids-based vesicles consisted of the following mono-unsaturated C18 acyl chains: 1,2-dioleoyl-*sn*-glycero-3-phosphocholine (DOPC), 1,2-dioleoyl-*sn*-glycero-3-phosphoethanolamine (DOPE) and 1,2-dioleoyl-*sn*-glycero-3-phosphoserine (DOPS). Cholesterol (Chol), SM and lyso-phospholipids as 1-oleoyl-2-hydroxy-*sn*-glycero-3-phosphocholine (LPC) and 1-oleoyl-2-hydroxy-*sn*-glycero-3-phosphoethanolamine (LPE) were also included in the formula. Molar ratios were DOPC (25)/DOPE (25)/DOPS (10)/Chol (25)/SM (10)/LPC (2.5)/LPE (2.5). The composition of the ether phospholipid-based vesicles (termed “nematode-like”) was comparable apart from the inclusion of 1-(1*Z*-octadecenyl)-2-oleoyl-*sn*-glycero-3-phosphoethanolamine (C18 plasmalogen-18:1 PE) in place of DOPE and a reduction in DOPC. Molar ratios were DOPC (5)/C18 (plasm)-18:1 PE (45)/DOPS (10)/Chol (25)/SM (10)/LPC (2.5)/LPE (2.5).

Results

Nematode exosomes are comparable in size and morphology to murine exosomes and share canonical exosomal markers

Transmission electron microscopy (TEM) was carried out to compare the size, shape and purity of exosomes isolated and purified from *H. polygyrus* excretory-secretory products (HES) and from the culture media of 2 different murine cell lines. As shown in Fig. 1a, exosomes from all 3 sources share similar morphology and size (in the range of 100 nm), though it is noted that the cup-shaped appearance can be an artefact of negative staining in TEM (28). As expected, the protein signatures of the murine exosomes are distinct to that of their producing cells, and the nematode exosomes display a distinct profile compared with EV-depleted secretory products (Fig. 1b). To further assess the purity of murine exosome preparations, we examined the expression of well-described markers ALIX and CD9. ALIX has been linked to exosome biogenesis from the MVBs, whereas CD9 is a member of the tetraspanin family of proteins (3). Figure 1c shows that both murine exosomes are enriched in these proteins in comparison to the whole cell lysates or EV-depleted supernatant from the parental cells. In contrast, β -actin shows a strong signal in cell lysates (Fig. 1c) and only a very weak signal in exosomes upon longer exposure (data not shown).

The profile of exosome proteins from the 2 murine cell lines appear more similar to one another as compared with the *H. polygyrus* exosomes (Fig. 1b, left panel), as might be expected. Our previous study identified highly enriched exosome-associated protein homologues in the *H. polygyrus* exosomes (compared with the rest of the secretion product) including ALIX, tetraspanin proteins, heat shock proteins and Rab protein family members (14). From further analysis of these mass spectrometric data, we have identified additional proteins highly enriched in nematode exosomes that are homologous to proteins previously described in mammalian exosomes and might be crucial for exosome biology (Table I). In particular, POD-1 is a coronin-like protein involved in *Caenorhabditis elegans* intracellular trafficking (endocytosis, phagocytosis), cellular polarization and architecture (34). RAL-1 is a Ras-related protein which mediates fusion events during lumenogenesis within *C. elegans* excretory cells [interestingly, its potential functional partner the ezrin-radixin-moesin protein (ERM-1) is also enriched in nematode exosomes] (35). Lastly Pgp-9 is enriched in the nematode exosomes and this is a permeability glycoprotein, which is known to be crucial for multidrug resistance and trafficking across membranes in other systems (36).

Differences in the surface charge of nematode versus mammalian-derived exosomes

Dynamic light scattering (DLS) measures the interactions (electrostatic repulsion or attraction forces) between particles present in a solution. This tool is often used to assess the size, charge and reproducibility of different preparations of liposomes or other nanoparticles (37–39). To highlight unique characteristics that might underpin differences in the properties of mammalian and nematode-derived exosomes, we performed DLS studies of their sizes and surface charges. The numerical values obtained, together with the polydispersity index (PdI) are summarized in Table II. The relatively low PdI measured for all EVs (0.33–0.46) is similar to what is described by others and is indicative of a relatively homogeneous preparation (40). The size distributions depicted in Fig. 2 show that murine and nematode-derived exosomes possess very similar average sizes (around 120 nm). One fundamental parameter known to affect the stability of particles in a solution is the Z-potential (surface charge) (41), which relates to how particles interact with one another and with the liquid in which they are dispersed. Systems with high Z-potential (± 30 mV) are generally considered to be stable such that the particles are well dispersed and present minimal flocculation (low viscosity). On the other hand, low Z-potential values (± 10 mV) are indicative of a less stable system where particles are not well dispersed showing a tendency to create aggregates (high viscosity). Figure 2 shows the Z-potential distribution of each exosome type. The murine exosome types display comparable

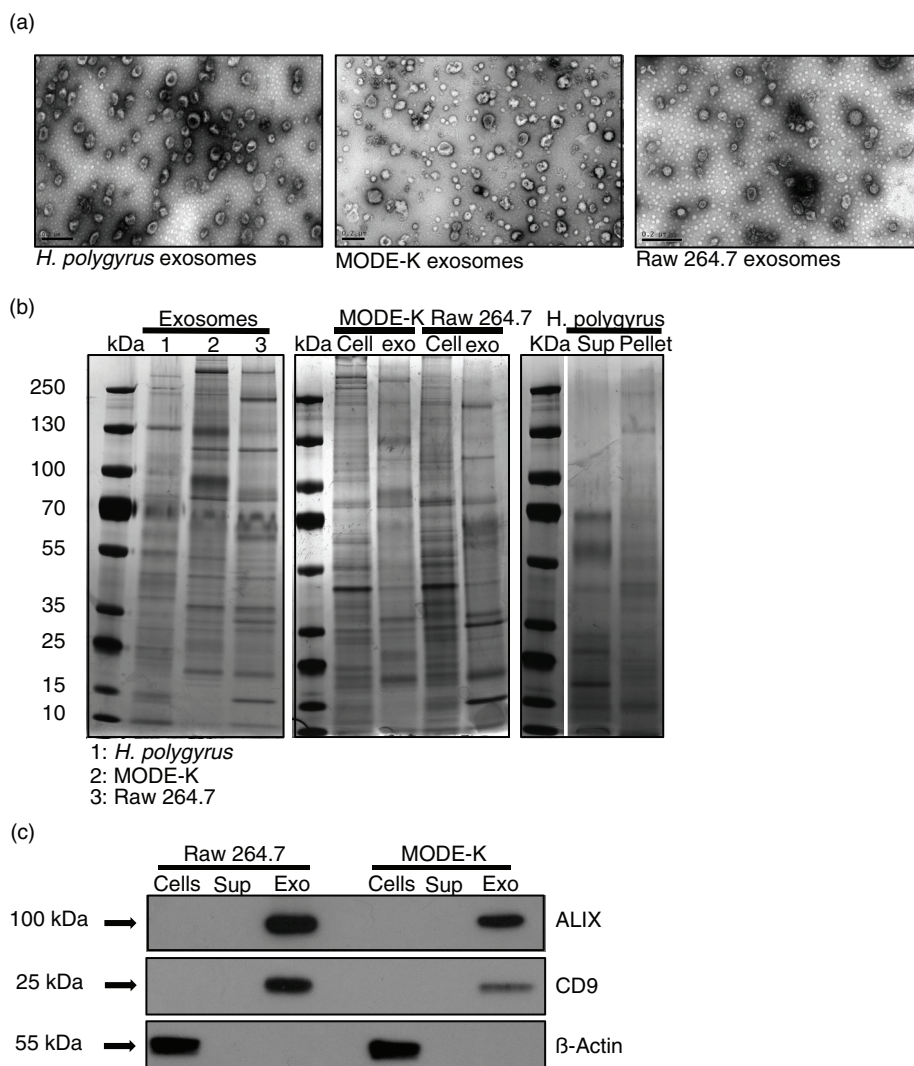


Fig. 1. Size, shape and protein profile of exosomes derived from the nematode compared with murine cell lines. (a) TEM images of exosomes from *H. polygyrus* (left panel), MODE-K cells (middle panel) and Raw 264.7 cells (right panel). Scale bar is 200 nm. (b) Protein profiles assessed by silver stain analysis of nematode exosomes compared with mammalian exosomes (left panel), mammalian exosomes compared with producing cell lysates (middle panel), and supernatant and pellet fractions following ultracentrifugation of *H. polygyrus* secretion product (right panel). (c) Western blot analysis of exosome-associated markers in the mouse ultracentrifugation products (supernatants and pellets) compared with the whole cell lysates. A total of 2 μ g protein was loaded on each gel for silver stain analysis and 3 μ g for western blot analysis. Arrows indicate closest ladder band with noted molecular weight.

surface charges; however, we measured a lower negative *Z*-potential for *H. polygyrus*-secreted vesicles. Very little is reported in the literature about DLS studies on

exosomes, but reports on neuroblastoma-derived exosomes show *Z*-potential values similar to those observed for nematode exosomes (40), whereas a different study on

Table 1. Mass spectrometric analysis of proteins highly enriched in HES pellet versus supernatant fraction (requiring ≥ 2 peptides detected) based on studies described in reference 14

<i>H. polygyrus</i> protein accession	BLAST homologue protein	Organism	Ratio P/S	p (n = 3)
Hp_I12366_IG04310_L3446	POD-1	<i>C. elegans</i>	168	<0.001
Hp_I14286_IG06230_L1419	RAL-1b	<i>C. elegans</i>	139	<0.001
Hp_I23793_IG15737_L576	Pgp-9	<i>C. elegans</i>	117	<0.001
Hp_I12527_IG04471_L2582	ERM-1	<i>C. elegans</i>	28	<0.001

Table II. Dynamic light scattering analysis of vesicle size and charge is reported together with the polydispersity index (Pdl)

Exosomes	Size (nm)	Pdl	Z-potential (mV)
<i>H. polygyrus</i>	122 ± 3	0.33 ± 0.11	-21.3 ± 1.56
MODE-K	122 ± 19	0.46 ± 0.03	-36.5 ± 2.89
Raw 264.7	111 ± 5	0.33 ± 0.11	-34.0 ± 0.56

exosomes from human cells reported larger negative Z-potential values of < -45 mV (42). As the surface charge is dependent on the protein and lipid composition of the membrane, further work is required to understand the nature of these differences and whether the lower negative charge impacts uptake properties (37).

Exosomes secreted by *H. polygyrus* contain high levels of ether-linked glycerophospholipids compared with mammalian exosomes

Lipidomic analysis was carried out for the nematode and murine exosomes based on extraction of glycerol-based phospholipids (PLs) and sphingolipids (SLs) as described in the Methods section. The compounds identified with their accurate mass measurement, elemental composition, calculated mass, error, double-bond equivalents and retention times are detailed in the Supplementary Table 1.

Glycerophospholipids

For the purpose of our study, the PLs were divided into 4 major classes: diacyl-PLs containing 2 ester-linked acyl chains (acyl fatty acids) at both the *sn-1* and *sn-2* positions of the glycerol, acyl lyso-PLs with just one acyl chain at the *sn-1* position, ether-PLs characterized by an ether-linked alkyl chain at the *sn-1* position of the glycerol and an acyl chain at the *sn-2* position, and finally ether lyso-PLs with just one alkyl chain at the *sn-1* position. Plasmalogens (Plsm) represent a particular subclass of ether lipids that are known to influence membrane dynamics and were reported to alter the fusion properties of synthetic vesicles (43,44). They have recently received increased interest due to their involvement in developmental and neurodegenerative diseases and inflammation (45). Here, the first carbon of the glycerol presents a vinyl-ether linked fatty alcohol (alkenyl chain) and the *sn-2* position is normally occupied by an unsaturated fatty acid, whereas the lyso-Plsm forms present just the alkenyl chain at the *sn-1* position. Due to their identical molecular formula and mass, it is challenging to distinguish between a plasmalogen (alkenyl-linked) and its correspondent alkyl-linked ether lipid; we, therefore, compared retention time and the mass spectrum of specific plasmalogen standards with those obtained from collected samples.

An overview of the total glycerol-based PL content from all 3 exosomes is provided in Fig. 3a with a breakdown of specific classes in Fig. 3b. In exosomes derived from murine cells, the most abundant species of diacyl-PLs are

phosphatidylcholine (PC, black) and phosphatidylserine (PS, green). In comparison, the amounts of these lipids are diminished in the nematode-derived exosomes (4 and 14% of total PLs, respectively), whereas the levels of diacyl phosphatidylethanolamine (PE, purple) are similar among all 3. It is worth noting, however, that the nematode exosomes globally contain higher levels of acyl lyso-PLs (Fig. 3a and Supplementary Fig. 1) though in proportion these species are much less abundant than non-lyso forms in all exosomes (< 10 -fold, Supplementary Table 2). In particular, the nematode exosomes have significantly higher levels of lyso-PS compared with the murine exosomes (2- and 2.4-fold change enrichment compared to MODE-K and Raw 264.7, respectively) as shown in Supplementary Fig. 1. Notably, all exosomes show a high content of ether-linked PLs (30% in mammalian exosomes and 62% in nematode exosomes, Fig. 3a and Supplementary Table 2). This is consistent with a recent report describing enrichment of ether lipids in exosomes from colorectal cancer cells, in which the authors also report high levels of Plsm-PE when compared with producing cells (16).

The nematode exosomes display significantly higher levels of ether-PE species (Fig. 3b, bottom panel). Most notably, the nematode exosomes show a striking enrichment in plasmalogen species (Fig. 3c). High levels of C36:2 Plsm-PE were detected (8.9- and 18.1-fold enrichment in nematode compared with MODE-K- and Raw 264.7-derived exosomes, respectively) together with high levels of C36:2 Plsm-PC (14.0- and 28.8-fold enrichment in nematode vs. MODE-K- and Raw 264.7-derived exosomes). These values are reported in Supplementary Table 3, which summarizes the ratios calculated from the raw data provided in Supplementary Table 2. Interestingly, the largest enrichments were measured for the lyso-Plsm forms. Specifically, C18:1 Plsm-LPE display a 62.4- and 56.3-fold enrichment in nematode versus MODE-K- and Raw 264.7-derived exosomes. A similar increase was detected in the C18:1 Plsm-LPC levels (60.1- and 30.1-fold change in nematode vs. MODE-K- and Raw 264.7-derived vesicles).

Sphingolipids

The levels of SM, ceramide (Cer), dihydrosphingomyelin (DHSM), dihydroceramide (DHCer) and ceramide monohexoside (CMH) were also measured following extraction from the same samples. SM is a major and ubiquitous component of cell membranes and has consistently been described as enriched in mammalian exosomes compared with their producing cells (18,19,46). Surprisingly, SM and DHSM levels were significantly decreased in nematode exosomes (nematode/mammalian SM ratio = 0.05, nematode/MODE-K and nematode/Raw 264.7 DHSM ratio = 0.6 and 0.4, respectively), as shown in Fig. 4a. Although SLs and SM in particular are

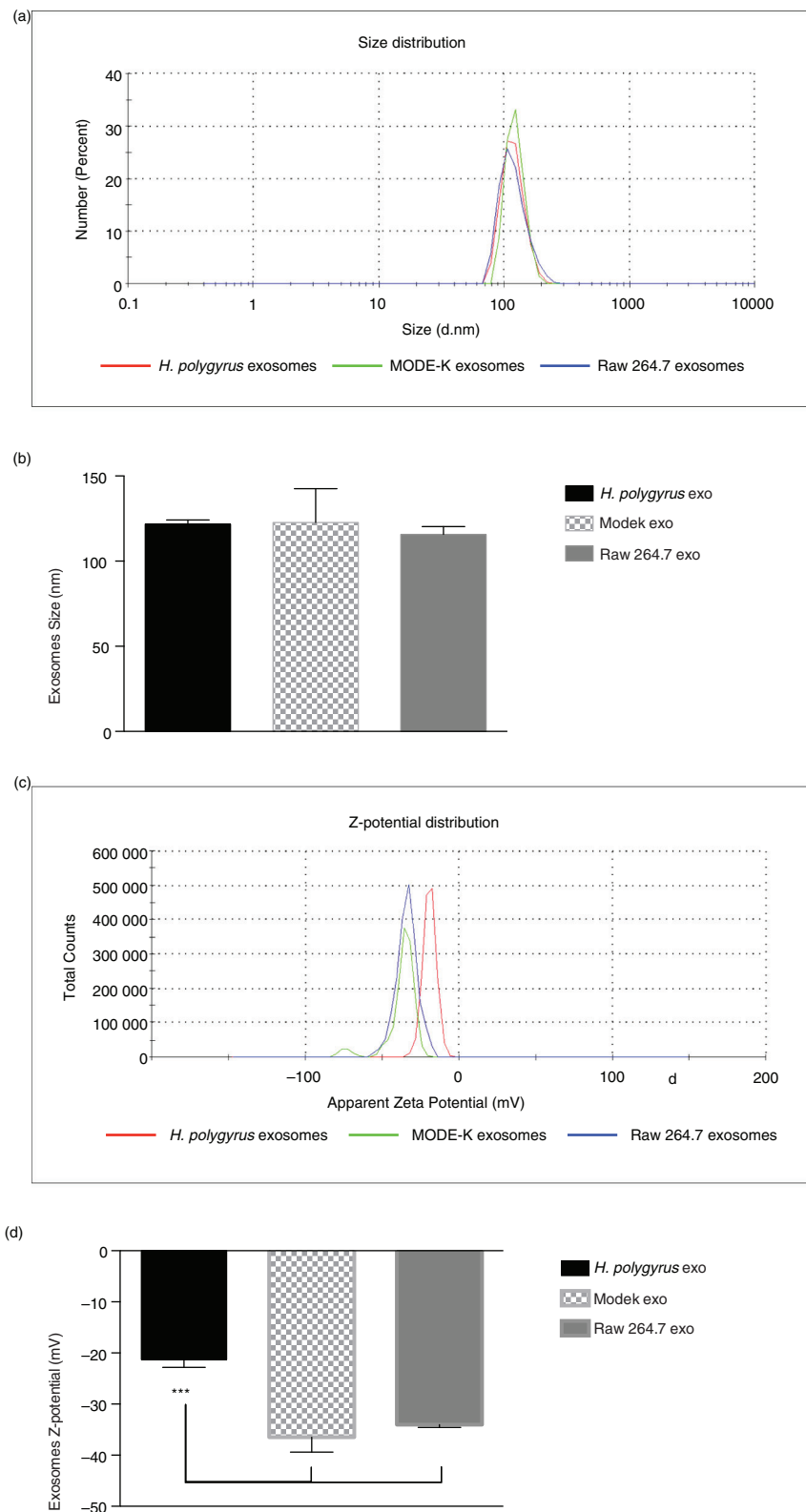


Fig. 2. Nematode exosomes have a similar size to murine exosomes but a significantly different surface charge. (a) Representative size distributions of exosomes and (b) average size from 3 biological replicates. (c) Representative zeta-potential distributions and (d) average zeta potential from 3 biological replicates. Results are based on dynamic light-scattering analysis using a zetasizer nano ZS90 particle sizer. A quantity of 5 µg exosome preparation (protein content) was used in each measurement. Results in (b and d) are shown as the mean ± SD, n = 3 biological replicates. ***p < 0.001 based on ANOVA, Tukey's multiple comparisons test.

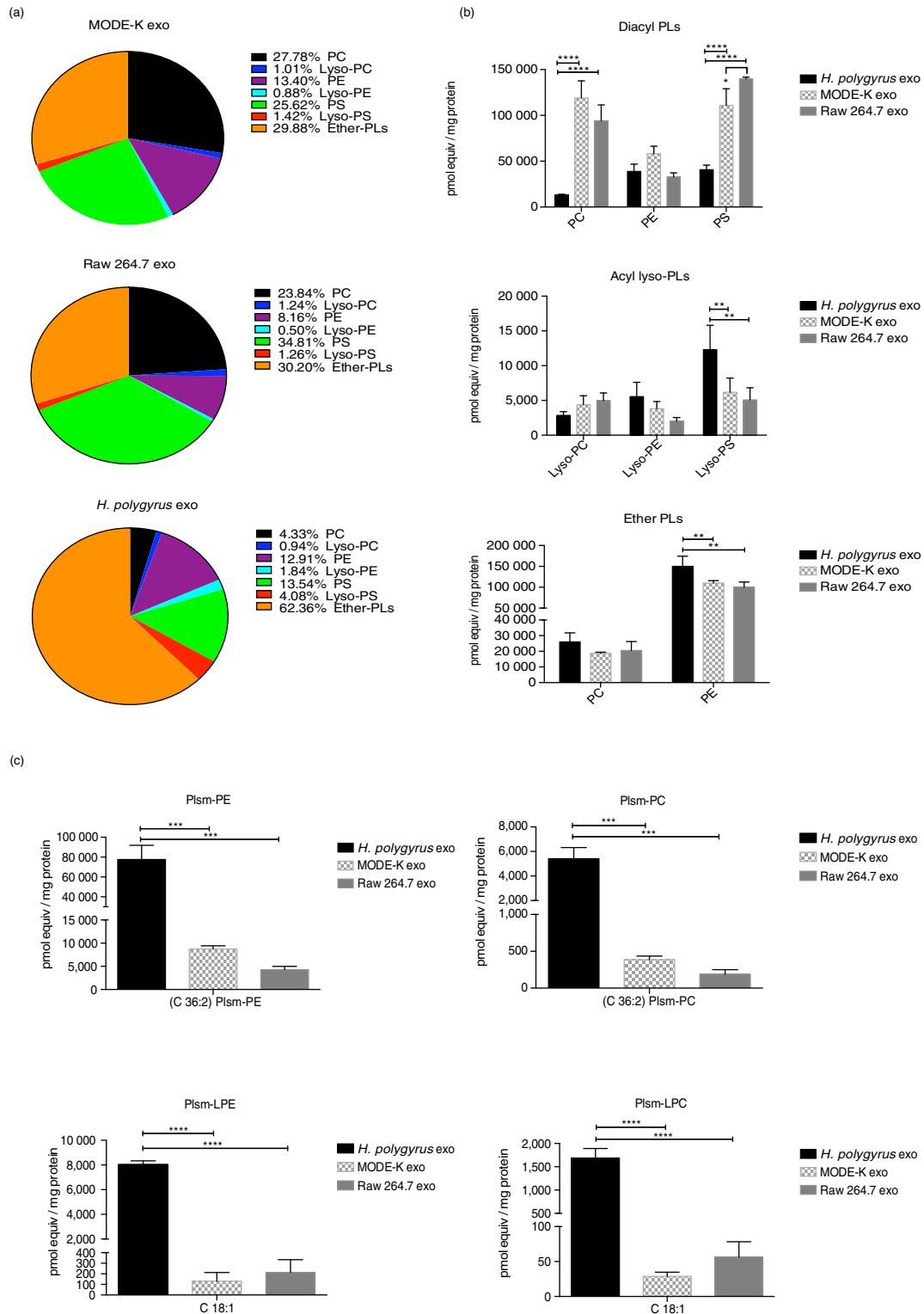


Fig. 3. Nematode-derived exosomes reveal a unique phospholipid profile compared with murine exosomes. (a) Overview of the global PL content of nematode and murine exosomes. Lipid classes are reported as a percentage of the total PL content. Ether-linked phospholipids (alkyl-acyl, lyso and alkenyl forms) are globally represented. Quantities of the major PLs classes (b) and plasmalogens (c) in nematode versus mouse exosomes. Data correspond to the mean \pm SD (n = 3 biological replicates for nematode- and MODE-K-derived exosomes and n = 2 biological replicates for Raw 264.7 exosomes). **p < 0.01, ***p < 0.001, ****p < 0.0001 based on ANOVA and Tukey's multiple comparisons test.

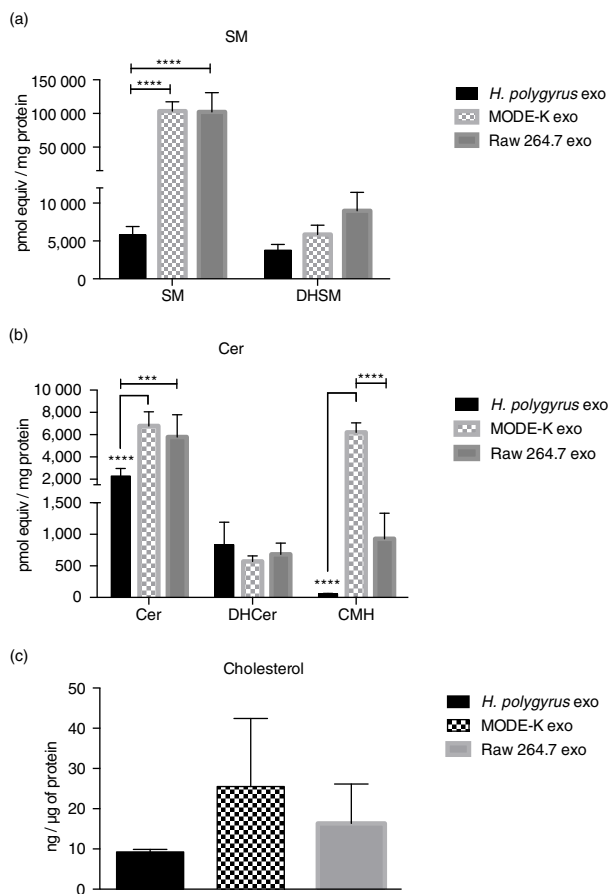


Fig. 4. Nematode-derived exosomes have reduced cholesterol and SM in comparison to murine exosomes. (a and b) Quantities of the SL classes in nematode and murine exosomes. Data correspond to the mean \pm SD (n = 3 biological replicates for nematode- and MODE-K-derived exosomes and n = 2 biological replicates for Raw 264.7 exosomes) (**p < 0.01, ***p < 0.001, ****p < 0.0001; ANOVA and Tukey's multiple comparisons test). (c) Cholesterol levels of nematode compared with murine exosomes assessed by the Amplex Red cholesterol assay kit using 3 μ g of exosomes (protein content) per measurement. Data represent the mean \pm SD with n = 3 biological replicates.

described as widely present in helminths, some discrepancies have been reported depending on the parasite species (26). In mammals, SM associates tightly with cholesterol at the plasma membrane and it is one of the key factors required for the assemblage of highly ordered and detergent-resistant micro-domains known as *lipids rafts* (22,47–49). It is therefore legitimate to speculate that nematode-derived exosomes might have evolved a different way to ensure rigidity and stability of their secreted vesicles. Similar to SM, higher levels of Cer have been consistently reported in mammalian exosomes compared with producing cells, where they may play a role in triggering exosome secretion by parental cells (50). Again, as shown in Fig. 4b, we found higher levels of Cer in

mammalian exosomes compared with those of nematodes. No significant differences were observed in terms of DHCer content, whereas the levels of more complex Cers were particularly high in MODE-K-derived exosomes, significantly diminished in Raw 264.7 and negligible in nematode exosomes.

Cholesterol

Together with SM, cholesterol has been described as highly enriched in exosomes from mammalian cells where it also contributes to exosome rigidity (18,23). However, as mentioned above, helminths are not able to synthesize cholesterol *de novo* and must obtain this from the environment and host. It is not clear whether cholesterol would therefore play the same role in exosomes secreted by these parasites. Here, we measured cholesterol content (free cholesterol and also cholesteryl esters) in nematode versus murine exosomes. The method used does not distinguish cholesterol in the vesicle membrane from that which could be within the lumen. As represented in Fig. 4c, nematode exosomes display lower levels of cholesterol/ μ g of protein than mammalian exosomes. Although not significant, this result fits with the low level of SM also observed in nematode exosomes. SM has been reported as a major factor driving cholesterol localization at the plasma membrane and depletion of plasma membrane SM results in cholesterol redistribution from the cell surface to intracellular membranes (51,52).

Nematode-derived exosomes have more rigid membranes than murine exosomes

We next aimed to determine whether the distinct lipid content of nematode and mammalian exosomes would translate into differences in membrane fluidity. To this end, studies were carried out with the lipophilic fluorescent dye Laurdan (2-dimethylamino-6-lauroyl-naphthalene), which intercalates into lipids bilayers and has different emission properties based on the degree of order of the environment (53,54). In a gel phase/ordered membrane where lipids are tightly packed, its emission spectrum peaks at 440 nm, whereas in a liquid/disordered phase the emission spectrum peaks at 490 nm. This 50 nm emission shift can therefore be quantified and used to distinguish between more-ordered gel-phase membranes and less-ordered liquid-phase membranes based on the generalized polarization (GP) index (55) according to $GP = (I_{440} - I_{490}) / (I_{440} + I_{490})$, where I_{440} and I_{490} are the maximum emission intensities registered in the gel and in the liquid-crystalline phase, respectively. The higher the GP index, the more tightly packed are the lipids and the more rigid is a membrane. As shown in Fig. 5a, *H. polygyrus*-derived exosomes exhibit significantly higher GP values compared with murine exosomes. Interestingly, we also detected a significant difference in the rigidity of exosomes secreted by MODE-K versus Raw 264.7 cells;

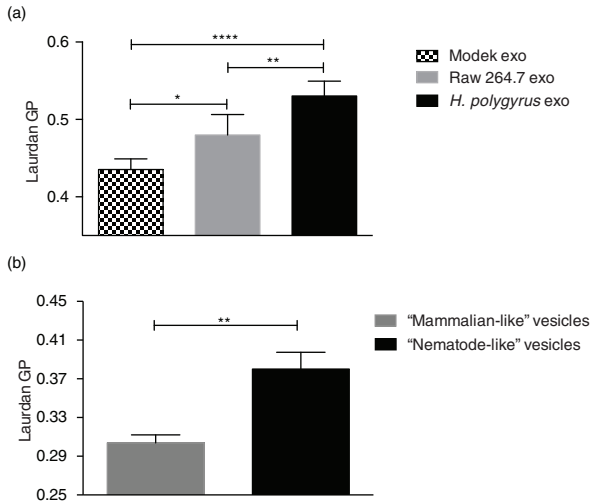


Fig. 5. Fluidity properties of exosomes and artificial vesicle membranes. (a) Laurdan GP values (at the maximum excitation wavelengths; 37°C) reveal higher rigidity for nematode compared with mammalian exosomes. Data are shown as mean \pm SD of 5 independent experiments performed using different biological replicates. (* $p < 0.05$, ** $p < 0.01$, *** $p < 0.001$, **** $p < 0.0001$; ANOVA and Tukey's multiple comparisons test). (b) "Nematode-like" artificial vesicles display higher GP values than "mammalian-like" vesicles. Data represent the mean \pm SD with $n = 3$ biological replicates. Data were acquired using the Fluoromax-3 Spectrofluorometer at 37°C. ** $p < 0.01$; Unpaired t-test with Welch's correction.

the latter being more rigid than the former. To date, there are only a handful of studies measuring exosomal membrane dynamics, but a previous report showed that exosomes released from cancer cells display higher GP values compared with exosomes secreted by healthy cells. The authors suggest that this increase in exosome rigidity is likely due to a different lipid composition and particularly to an enrichment in cholesterol, SM and gangliosides that occurs when the producing cells are exposed to an acidic pH, as in a tumour-like microenvironment (33). However, the higher rigidity that we observe for nematode exosomes seems to be in contrast to the lower levels of SM and cholesterol detected in their membranes.

Ether glycerophospholipids provide rigidity to nematode exosomes but have no impact on their fusion efficiency

According to the results above, the nematode exosomes display increased rigidity compared with those secreted by murine cells, but this cannot be attributed to cholesterol or SM levels, which are in fact decreased in the nematode exosomes. To determine whether the increased levels of ether-linked PE (and specifically, the plasmalogen species) could account for increased rigidity, we used custom artificial vesicles in which the lipid contents were tailored to compare the high content of plasmalo-

gens observed in nematode-derived vesicles with the lower levels in mammalian vesicles. Specifically, 2 sets of vesicle were made: "nematode-like" which contained increased levels of ether-PE (45% of C18 Plsm-PE) with a concomitant decrease in diacyl-PC contents (down to 5%) and "mammalian-like" containing 25% of the correspondent diacyl-PE and 25% of diacyl-PC. The levels of the remaining lipids used in the formula such as diacyl-PS, lyso-PLs (lyso-PC and lyso-PE), SM and cholesterol were identical in both vesicles as described in Methods. As shown in Fig. 5b, the nematode-like artificial vesicles show a significantly higher GP value than the mammalian-like control vesicles. These data demonstrate that beyond SM and cholesterol, high levels of plasmalogens in a lipid bilayer can create a more rigid membrane and provide a rationale for why these might be enriched in *H. polygyrus* exosomes. These results are in agreement with the previous reports on the role of ether-PE and plasmalogen species increasing the rigidity of membranes (56,57), although this had not previously been examined in EVs.

Analogously, previous studies have also shown that Plsm-PE can stabilize membranes and promote fusion events in synaptic vesicles and in vitro models of artificial vesicles (43,58,59). We therefore set out to examine the fusion properties of the nematode exosomes in comparison to those derived from murine cells using the lipophilic self-quenching fluorescent dye octadecyl rhodamine B chloride (R18). The dye is incorporated into lipid bilayers and increases its fluorescence (fluorescence de-quenching, FD) upon dilution caused by fusion of the bilayer with other membranes. The exosomes were fluorescently labelled with the R18 dye and incubated with mouse small intestine epithelial cells (MODE-K cell line). We previously showed that *H. polygyrus* exosomes are internalized by these cells, and this cell type is expected to be in close proximity to the adult nematode in vivo (14). Fluorescence de-quenching was monitored over a 30-min time frame at physiological temperature, and the reaction was stopped by the addition of Triton X-100 in order to lyse the vesicles and measure the maximum fluorescence de-quenching. Results in Fig. 6a show the dramatic increase in the fluorescence following the addition of cells in contrast to the steady fluorescence observed prior to incubation. When the % FD was calculated taking into account the initial fluorescence F_i (of the labelled vesicles) and the final fluorescence F_{max} (after addition of Triton X-100), no significant differences were registered between each exosome type (Fig. 6b). In fact, all exosomes show a very similar % FD curve reaching about 10% of the maximum fluorescence de-quenching obtained with Triton X-100. These data suggest that although nematode exosomes maintain a rigid structure that is likely related to their high level of ether lipids, they do not display superior fusion properties with these murine cells. In contrast,

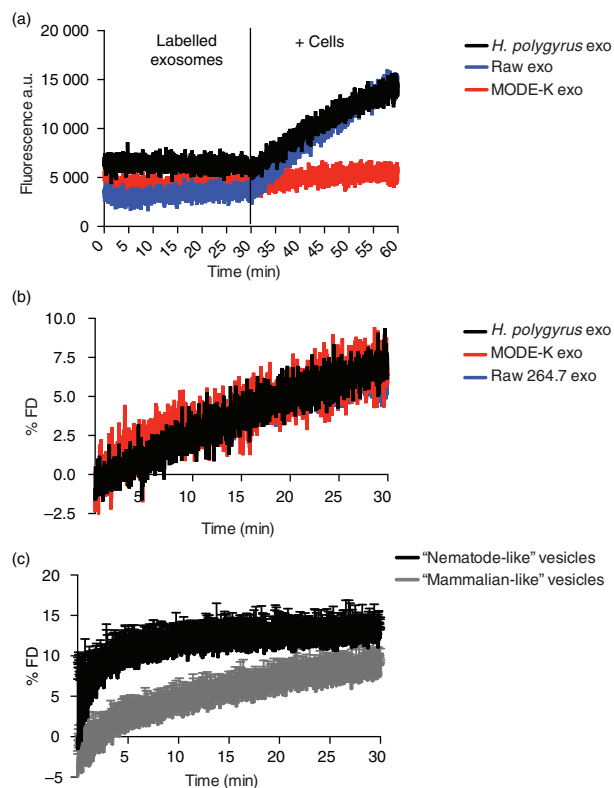


Fig. 6. Membrane fusion efficiency studies. Exosomes were labelled using the R18 self-quenching dye as described in the Methods section. After 30-min equilibration time, labelled vesicles were mixed with 1×10^6 live MODE-K cells and the de-quenching of the fluorescence was monitored continuously, using the Fluoromax-3 spectrofluorometer. The reaction was stopped by the addition of Triton X-100. The fusion efficiency was expressed as % of R18 fluorescence de-quenching (% FD). (a) De-quenching increase of the fluorescence upon fusion of labelled vesicles with live cells. (b) Nematode exosomes show no difference in fusion efficiency compared with murine exosomes. (c) “Nematode-like” artificial vesicles with high content of plasmalogens are more fusionogenic than “mammalian-like” vesicles with correspondent acyl-lipids. Values are the mean \pm SD of 3 independent experiments. Data correspond to one representative experiment of 3 with similar results.

analysis of the fusion properties of the artificial vesicles demonstrates that the elevated levels of ether lipids present in the nematode-like vesicles result in a higher fusionogenic profile compared with mammalian-like vesicles containing acyl-based lipids (Fig. 6c). It seems likely therefore that additional factors beyond membrane rigidity have a larger influence on the interaction of exosomes with recipient cells (60). This is perhaps not surprising considering the complexity of the exosome proteomes and the fact that proteins and glycoproteins are also likely involved in uptake. Further work is required to understand whether the distinct lipid content of nematode exosomes alters any aspects of their recognition, uptake and internalization into host cells.

Discussion

This work uses a biochemical and lipid-focused approach to compare exosomes secreted by a nematode parasite with those secreted by cells of its mouse host. We use the term “exosome” based on the size and protein markers of the EVs we characterize; however, we note that there is scope for heterogeneity in the exact composition of EVs within the populations we have isolated. Consistent with previous reports, we demonstrate that nematode-derived exosomes are similar in shape and appearance to mammalian exosomes with a number of homologous proteins. We also identify 4 additional proteins of interest in the nematode exosomes with potential implications in vesicle trafficking, fusion events, transport of xenobiotics and protection of exosomal content upon internalization. Specifically, POD-1 is involved in *C. elegans* intracellular trafficking, cellular polarization and architecture (34). The expression of its homologue protein, Coronin-1, in macrophages prevents the fusion of the phagosomes with degradative lysosomes (61–64) and might similarly have a protective role for exosome cargo. RAL-1 is a Ras-related protein which mediates cytoplasmic vesicle fusion during the lumenogenesis within *C. elegans* excretory cells (35). Interestingly, we found that its potential functional partner the ERM-1 is also enriched in nematode exosomes. Lastly, Pgp-9 is homologue to mammalian permeability glycoproteins, previously described in mammalian exosomes as involved in transfer of drug resistance from resistant breast cancer cells to sensitive ones (65). This protein has been reported to play a major role in mediating anthelmintic drug resistance (66); whether parasite-derived EVs are involved in this resistance is unknown.

Biophysical characterization of *H. polygyrus* exosomes reveals distinct features compared with murine exosomes, including a less negative surface charge and higher membrane rigidity. In cell membranes, SM and cholesterol are known to be tightly associated in lipid rafts and play an important role in membrane structure, rigidity and trafficking (22,47). Importantly, mammalian exosomes have been shown to have enriched levels of these lipids when compared with producing cells, and the presence of raft-like domains has been extensively described in exosomes where they appear to contribute to sorting of exosome proteins (67,68). However, both lipid species were decreased in overall abundance in the nematode exosomes and nematodes do not synthesize their own cholesterol but must obtain this from the environment. Rather, global lipidomic analysis revealed a striking enrichment of ether-linked PLs in the nematode exosomes compared with those from mouse cells. Previously, Llorente et al. (20) identified enrichment of one species of ether-PLs (18:1 ether-PE) in exosomes released from a metastatic prostate cancer cell line compared with parental cells. A year later, the same group described how treatment of PC-3 cells with an

ether-lipid precursor causes alteration in exosomal lipid and protein composition and results in enhanced exosome release (69), although the mechanism for this is not known. Little is known about regulation of secretion of vesicles in nematodes including the role of ether lipids and whether the availability of cholesterol from the environment/host also influences EVs produced from these parasites.

Our results show that 30% of the global PL content of exosomes secreted from both epithelial and macrophage mouse cells is represented by ether-linked species. This agrees with a recent report on exosomes secreted by colorectal cancer cells, showing a high content of ether-linked PLs when compared with producing cells. In the same study, the authors also reported particularly high levels of Plsm-PE (16). We show here that nematode-derived vesicles are especially enriched in ether-linked lipids (comprising 62% of the total PL content) and particularly, in comparison to murine exosomes, they display a significant increase in the ether-PE species. In addition, nematode exosomes show a striking enrichment in plasmalogen levels. Using studies with synthetic vesicles containing different amounts of plasmalogens, we show that this class of lipid increases the rigidity of vesicle membranes, in agreement with its reported role in altering membrane properties and fluidity (56,57). We speculate that the high levels of plasmalogens in nematode exosomes might therefore mediate an increased stability of the vesicles within the harsh mouse intestinal milieu. Furthermore, Plsm-PE has been previously described to facilitate membrane fusion events in synaptic vesicles as well as artificial vesicles (43,58,59). Our own studies are consistent with this in the case of the artificial vesicles; however, we do not see increased fusion rates or higher efficiency in the cellular internalization of nematode exosomes compared with those derived from mammalian cells. This is not necessarily surprising as multiple uptake pathways for EVs have been suggested including direct lipid and/or protein-mediated fusion, receptor-dependent or independent endocytosis or phagocytosis, which are enacted depending on cell type and other stimuli (60). Further studies are needed to better understand the mechanisms that lead to internalization of exosomes, along with the roles of lipids in these processes.

In mammals, plasmalogens normally represent about 15–20% of the total PL content in cell membranes but their expression varies among different tissues. In humans, PE-plasmalogen levels are particularly enriched ($\geq 50\%$ of total PE fraction) in brain, heart, kidney, skeletal muscle, neutrophils and eosinophils (45). Remarkably, PE plasmalogens represent almost 90% of the total PE fraction in myelin, whereas their levels have been described to decrease with ageing and in neurodegenerative disorders such as Alzheimer's disease (70–72) suggesting their potential importance in vesicle-mediated signal transduction.

Relatively little has been reported about plasmalogens in helminths or other invertebrates (73) but high levels of Plsm-PE were found in the outer tegumental membrane of *Schistosoma mansoni*, where they account for 44% of the total PE content (74). The authors suggest that the high plasmalogen content might modulate the activity of specific parasite membrane-associated proteins helping to protect against the host immune response. A similar enrichment in PE plasmalogens has also been described in the nematode plant parasite *Meloidogyne javanica* (75) and in the free-living nematode *Turbatrix aceti* (76) where the levels of PE plasmalogens represent 53% of the total PE content. Our work reports high levels of plasmalogens in exosomal membranes, and to date is the only lipidomic characterization of exosomes derived from a helminth parasite.

We also detected enriched levels of lyso-PS in the exosomes secreted by *H. polygyrus* compared with those derived from murine cells. Lyso-PLs represent another class of lipids that have been scarcely characterized in exosomes with variable findings depending on the cell type from which they originate (19,20,77,78). A previous report demonstrated that lyso-PS extracted from the tegument of *S. mansoni* activates TLR2 and affects DC polarization. Importantly, this effect on TLR2 was specifically mediated by the parasite lyso-PS species, as neither a commercial synthetic nor a mammalian-derived lyso-PS had any effect on TLR2 activation (79).

It is intriguing to consider the possible immunomodulatory functions of exosome lipids, an area largely unexplored. In this regard, the high levels of plasmalogens observed in *H. polygyrus* exosomes could also mediate the production in the host of second messenger lipids involved in signal transduction and inflammation such as arachidonic acid and prostaglandins. Differential use in the catabolism of plasmalogens by specific phospholipases might play a role in mediating the specificity of the process (57,80). Overall, these results demonstrate that exosomes secreted by the nematode parasite *H. polygyrus*, although sharing similarities with mammalian exosomes, display a unique lipid content along with differences in surface charge and membrane fluidity. These distinctive attributes might be crucial for the parasite exosomes to mediate an efficient interaction with their environment and host cells.

Availability of data and materials

All of the lipidomic data are provided in Supplementary Table 2 and will be deposited into Vesiclepedia (www.microvesicles.org/) upon acceptance of the manuscript.

Authors' contributions

FS designed and performed lipidomic and biochemical experiments and drafted manuscript, JMC co-designed and assisted with DLS experiments, GC, MM and RMM provided support for the *H. polygyrus* life cycle

and helpful suggestions, JC and GF co-designed and co-analysed lipidomic data with FS, AHB conceived of initial project, supervised biochemical studies and co-wrote/edited final manuscript with FS. All authors read and approved the final manuscript.

Acknowledgements

We thank Phil Whitfield and Mary Doherty for helpful discussions at the start of this project. We also thank Eva Dalmau Alsina for helping with sample preparation and injection into UPLC–MS/MS equipment. We thank Mark Bradley for use of the Zetasizer and Liz Blackburn for the use of the FluoroMax-3.

Conflict of interest and funding

The authors have not received any funding or benefits from industry or elsewhere to conduct this study. The project was supported by Wellcome Trust RCDF to A. Buck (WT097394A1A) and Wellcome Trust strategic award to the Centre for Immunity, Infection & Evolution (WT095831).

References

- Raposo G, Stoorvogel W. Extracellular vesicles: exosomes, microvesicles, and friends. *J Cell Biol.* 2013;200:373–83.
- Fevrier B, Raposo G. Exosomes: endosomal-derived vesicles shipping extracellular messages. *Curr Opin Cell Biol.* 2004; 16:415–21.
- Colombo M, Raposo G, Thery C. Biogenesis, secretion, and intercellular interactions of exosomes and other extracellular vesicles. *Annu Rev Cell Dev Biol.* 2014;30:255–89.
- Johnstone RM, Adam M, Hammond JR, Orr L, Turbide C. Vesicle formation during reticulocyte maturation. Association of plasma membrane activities with released vesicles (exosomes). *J Biol Chem.* 1987;262:9412–20.
- Pan BT, Johnstone RM. Fate of the transferrin receptor during maturation of sheep reticulocytes in vitro: selective externalization of the receptor. *Cell.* 1983;33:967–78.
- Harding C, Heuser J, Stahl P. Receptor-mediated endocytosis of transferrin and recycling of the transferrin receptor in rat reticulocytes. *J Cell Biol.* 1983;97:329–39.
- Raposo G, Nijman HW, Stoorvogel W, Liejendekker R, Harding CV, Melief CJ, et al. B lymphocytes secrete antigen-presenting vesicles. *J Exp Med.* 1996;183:1161–72.
- De Toro J, Herschlik L, Waldner C, Mongini C. Emerging roles of exosomes in normal and pathological conditions: new insights for diagnosis and therapeutic applications. *Front Immunol.* 2015;6:203.
- Marcilla A, Martin-Jaular L, Trelis M, de Menezes-Neto A, Osuna A, Bernal D, et al. Extracellular vesicles in parasitic diseases. *J Extracell Vesicles.* 2014;3:25040, doi: <http://dx.doi.org/10.3402/jev.v3.25040>
- Coakley G, Maizels RM, Buck AH. Exosomes and other extracellular vesicles: the new communicators in parasite infections. *Trends Parasitol.* 2015;31:477–89.
- Mu JY, Zhuang XY, Wang QL, Jiang H, Deng ZB, Wang BM, et al. Interspecies communication between plant and mouse gut host cells through edible plant derived exosome-like nanoparticles. *Mol Nutr Food Res.* 2014;58:1561–73.
- Ju S, Mu J, Dokland T, Zhuang X, Wang Q, Jiang H, et al. Grape exosome-like nanoparticles induce intestinal stem cells and protect mice from DSS-induced colitis. *Mol Ther.* 2013;21:1345–57.
- Regente M, Pinedo M, Elizalde M, de la Canal L. Apoplastic exosome-like vesicles: a new way of protein secretion in plants? *Plant Signal Behav.* 2012;7:544–6.
- Buck AH, Coakley G, Simbari F, McSorley HJ, Quintana JF, Le Bihan T, et al. Exosomes secreted by nematode parasites transfer small RNAs to mammalian cells and modulate innate immunity. *Nat Commun.* 2014;5:5488.
- Kalra H, Simpson RJ, Ji H, Aikawa E, Altevogt P, Askenase P, et al. Vesiclepedia: a compendium for extracellular vesicles with continuous community annotation. *PLoS Biol.* 2012; 10:e1001450.
- Lydic TA, Townsend S, Adda CG, Collins C, Mathivanan S, Reid GE. Rapid and comprehensive “shotgun” lipidome profiling of colorectal cancer cell derived exosomes. *Methods.* 2015;87:83–95.
- Carayon K, Chaoui K, Ronzier E, Lazar I, Bertrand-Michel J, Roques V, et al. Proteolipidic composition of exosomes changes during reticulocyte maturation. *J Biol Chem.* 2011; 286:34426–39.
- Wubbolts R, Leckie RS, Veenhuizen PT, Schwarzmann G, Mobius W, Hoernschemeyer J, et al. Proteomic and biochemical analyses of human B cell-derived exosomes. Potential implications for their function and multivesicular body formation. *J Biol Chem.* [Research Support, Non-U.S. Gov't]. 2003; 278:10963–72.
- Laulagnier K, Motta C, Hamdi S, Roy S, Fauvelle F, Pageaux JF, et al. Mast cell- and dendritic cell-derived exosomes display a specific lipid composition and an unusual membrane organization. *Biochem J.* 2004;380(Pt 1):161–71.
- Llorente A, Skotland T, Sylvanne T, Kauhanen D, Rog T, Orłowski A, et al. Molecular lipidomics of exosomes released by PC-3 prostate cancer cells. *Biochim Biophys Acta.* 2013;1831:1302–9.
- Yanez-Mo M, Siljander PR, Andreu Z, Zavec AB, Borrás FE, Buzas EI, et al. Biological properties of extracellular vesicles and their physiological functions. *J Extracell Vesicles.* 2015;4:27066, doi: <http://dx.doi.org/10.3402/jev.v4.27066>
- Barenholz Y. Sphingomyelin and cholesterol: from membrane biophysics and rafts to potential medical applications. *Subcell Biochem.* 2004;37:167–215.
- Record M, Carayon K, Poirot M, Silvente-Poirot S. Exosomes as new vesicular lipid transporters involved in cell-cell communication and various pathophysiological processes. *Biochim Biophys Acta.* 2014;1841:108–20.
- Chitwood DJ, Lusby WR. Metabolism of plant sterols by nematodes. *Lipids.* 1991;26:619–27.
- Lee DL. The biology of nematodes. London: Taylor & Francis; 2002.
- Bankov I, Timanova A, Barrett J. Sphingomyelin synthesis in helminths: a minireview. *Folia Parasitol (Praha).* 1998;45: 257–60.
- Johnston CJ, Robertson E, Harcus Y, Grainger JR, Coakley G, Smyth DJ, et al. Cultivation of *Heligmosomoides polygyrus*: an immunomodulatory nematode parasite and its secreted products. *J Vis Exp.* 2015;98:e52412.
- Thery C, Amigorena S, Raposo G, Clayton A. Isolation and characterization of exosomes from cell culture supernatants and biological fluids. *Curr Protoc Cell Biol.* 2006; Chapter 3: Unit 3 22.
- Vidal K, Grosjean I, evillard JP, Gespach C, Kaiserlian D. Immortalization of mouse intestinal epithelial cells by the SV40-large T gene. Phenotypic and immune characterization of the MODE-K cell line. *J Immunol Methods.* 1993;166: 63–73.
- Garanto A, Mandal NA, Egidio-Gabas M, Marfany G, Fabrias G, Anderson RE, et al. Specific sphingolipid content decrease

- in Cerkl knockdown mouse retinas. *Exp Eye Res.* 2013;110:96–106.
31. Gorrochategui E, Casas J, Perez-Albaladejo E, Jauregui O, Porte C, Lacorte S. Characterization of complex lipid mixtures in contaminant exposed JEG-3 cells using liquid chromatography and high-resolution mass spectrometry. *Environ Sci Pollut Res Int.* 2014;21:11907–16.
 32. Palleschi S, Silvestroni L. Laurdan fluorescence spectroscopy reveals a single liquid-crystalline lipid phase and lack of thermotropic phase transitions in the plasma membrane of living human sperm. *Biochim Biophys Acta.* 1996;1279:197–202.
 33. Parolini I, Federici C, Raggi C, Lugini L, Palleschi S, De Milito A, et al. Microenvironmental pH is a key factor for exosome traffic in tumor cells. *J Biol Chem.* 2009;284:34211–22.
 34. Rappleye CA, Paredez AR, Smith CW, McDonald KL, Aroian RV. The coronin-like protein POD-1 is required for anterior–posterior axis formation and cellular architecture in the nematode *Caenorhabditis elegans*. *Genes Dev.* 1999;13:2838–51.
 35. Armenti ST, Chan E, Nance J. Polarized exocyst-mediated vesicle fusion directs intracellular lumenogenesis within the *C. elegans* excretory cell. *Dev Biol.* 2014;394:110–21.
 36. Aller SG, Yu J, Ward A, Weng Y, Chittaboina S, Zhuo R, et al. Structure of P-glycoprotein reveals a molecular basis for poly-specific drug binding. *Science.* 2009;323:1718–22.
 37. Roger E, Lagarce F, Benoit JP. The gastrointestinal stability of lipid nanocapsules. *Int J Pharm.* 2009;379:260–5.
 38. Honary S, Zahir F. Effect of zeta potential on the properties of nano-drug delivery systems – a review (Part 1). *Trop J Pharm Res.* 2013;12:255–64.
 39. Honary S, Zahir F. Effect of zeta potential on the properties of nano-drug delivery systems – a review (Part 2). *Trop J Pharm Res.* 2013;12:265–73.
 40. Marimpietri D, Petretto A, Raffaghello L, Pezzolo A, Gagliani C, Tacchetti C, et al. Proteome profiling of neuroblastoma-derived exosomes reveal the expression of proteins potentially involved in tumor progression. *PLoS One.* 2013;8:e75054.
 41. Kaszuba M, Corbett J, Watson FM, Jones A. High-concentration zeta potential measurements using light-scattering techniques. *Philos Trans A Math Phys Eng Sci.* 2010;368:4439–51.
 42. Sokolova V, Ludwig AK, Hornung S, Rotan O, Horn PA, Epple M, et al. Characterisation of exosomes derived from human cells by nanoparticle tracking analysis and scanning electron microscopy. *Colloids Surf B Biointerfaces.* 2011;87:146–50.
 43. Lohner K, Balgavy P, Hermetter A, Paltauf F, Lagner P. Stabilization of non-bilayer structures by the etherlipid ethanolamine plasmalogen. *Biochim Biophys Acta.* 1991;1061:132–40.
 44. Lohner K. Is the high propensity of ethanolamine plasmalogens to form non-lamellar lipid structures manifested in the properties of biomembranes? *Chem Phys Lipids.* 1996;81:167–84.
 45. Braverman NE, Moser AB. Functions of plasmalogen lipids in health and disease. *Biochim Biophys Acta.* 2012;1822:1442–52.
 46. Subra C, Laulagnier K, Perret B, Record M. Exosome lipidomics unravels lipid sorting at the level of multivesicular bodies. *Biochimie.* 2007;89:205–12.
 47. Ito J, Nagayasu Y, Yokoyama S. Cholesterol–sphingomyelin interaction in membrane and apolipoprotein-mediated cellular cholesterol efflux. *J Lipid Res.* 2000;41:894–904.
 48. Sonnino S, Prinetti A. Membrane domains and the “lipid raft” concept. *Curr Med Chem.* 2013;20:4–21.
 49. Ikonen E. Roles of lipid rafts in membrane transport. *Curr Opin Cell Biol.* 2001;13:470–7.
 50. Trajkovic K. Ceramide triggers budding of exosome vesicles into multivesicular endosomes. *Science.* 2008;319:1244–7.
 51. Slotte JP, Hedstrom G, Rannstrom S, Ekman S. Effects of sphingomyelin degradation on cell cholesterol oxidizability and steady-state distribution between the cell-surface and the cell interior. *Biochim Biophys Acta.* 1989;985:90–6.
 52. Harmala AS, Porn MI, Mattjus P, Slotte JP. Cholesterol transport from plasma-membranes to intracellular membranes is inhibited by 3-beta-[2-(diethylamino)ethoxy]androst-5-en-17-one. *Biochim Biophys Acta.* 1994;1211:317–25.
 53. Weber G, Farris FJ. Synthesis and spectral properties of a hydrophobic fluorescent probe: 6-propionyl-2-(dimethylamino) naphthalene. *Biochemistry.* 1979;18:3075–8.
 54. Parasassi T, Gratton E. Membrane lipid domains and dynamics as detected by Laurdan fluorescence. *J Fluoresc.* 1995;5:59–69.
 55. Sanchez SA, Triccerri MA, Gratton E. Laurdan generalized polarization fluctuations measures membrane packing micro-heterogeneity in vivo. *Proc Natl Acad Sci USA.* 2012;109:7314–9.
 56. Han XL, Gross RW. Plasmenylcholine and phosphatidylcholine membrane bilayers possess distinct conformational motifs. *Biochemistry.* 1990;29:4992–6.
 57. Paltauf F. Ether lipids in biomembranes. *Chem Phys Lipids.* 1994;74:101–39.
 58. Breckenridge WC, Morgan IG, Zanetta JP, Vincendon G. Adult rat brain synaptic vesicles. II. Lipid composition. *Biochim Biophys Acta.* 1973;320:681–6.
 59. Glaser PE, Gross RW. Plasmenylethanolamine facilitates rapid membrane fusion: a stopped-flow kinetic investigation correlating the propensity of a major plasma membrane constituent to adopt an HII phase with its ability to promote membrane fusion. *Biochemistry.* 1994;33:5805–12.
 60. Mulcahy LA, Pink RC, Carter DR. Routes and mechanisms of extracellular vesicle uptake. *J Extracell Vesicles.* 2014;3:24641, doi: <http://dx.doi.org/10.3402/jev.v3.24641>
 61. Jayachandran R, BoseDasgupta S, Pieters J. Surviving the macrophage: tools and tricks employed by *Mycobacterium tuberculosis*. *Curr Top Microbiol Immunol.* 2013;374:189–209.
 62. Jayachandran R, Sundaramurthy V, Combaluzier B, Mueller P, Korf H, Huygen K, et al. Survival of mycobacteria in macrophages is mediated by coronin 1-dependent activation of calcineurin. *Cell.* 2007;130:37–50.
 63. Pieters J, Muller P, Jayachandran R. On guard: coronin proteins in innate and adaptive immunity. *Nat Rev Immunol.* 2013;13:510–8.
 64. Zheng PY, Jones NL. *Helicobacter pylori* strains expressing the vacuolating cytotoxin interrupt phagosome maturation in macrophages by recruiting and retaining TACO (coronin 1) protein. *Cell Microbiol.* 2003;5:25–40.
 65. Lv MM, Zhu XY, Chen WX, Zhong SL, Hu Q, Ma TF, et al. Exosomes mediate drug resistance transfer in MCF-7 breast cancer cells and a probable mechanism is delivery of P-glycoprotein. *Tumor Biol.* 2014;35:10773–9.
 66. Lespine A, Menez C, Bourguinat C, Prichard RK. P-glycoproteins and other multidrug resistance transporters in the pharmacology of anthelmintics: prospects for reversing transport-dependent anthelmintic resistance. *Int J Parasitol Drugs Drug Resist.* 2012;2:58–75.
 67. de Gassart A, Geminard C, Fevrier B, Raposo G, Vidal M. Lipid raft-associated protein sorting in exosomes. *Blood.* 2003;102:4336–44.
 68. Valapala M, Vishwanatha JK. Lipid raft endocytosis and exosomal transport facilitate extracellular trafficking of annexin A2. *J Biol Chem.* 2011;286:30911–25.
 69. Phuyal S, Skotland T, Hessvik NP, Simolin H, Overbye A, Brech A, et al. The ether lipid precursor hexadecylglycerol stimulates

- the release and changes the composition of exosomes derived from PC-3 cells. *J Biol Chem*. 2015;290:4225–37.
70. Han XL, Holtzman DM, McKeel DW. Plasmalogen deficiency in early Alzheimer's disease subjects and in animal models: molecular characterization using electrospray ionization mass spectrometry. *J Neurochem*. 2001;77:1168–80.
 71. Farooqui AA, Horrocks LA. Plasmalogens: workhorse lipids of membranes in normal and injured neurons and glia. *Neuroscientist*. 2001;7:232–45.
 72. Maeba R, Maeda T, Kinoshita M, Takao K, Takenaka H, Kusano J, et al. Plasmalogens in human serum positively correlate with high-density lipoprotein and decrease with aging. *J Atheroscler Thromb*. 2007;14:12–8.
 73. Sugiura T, Fukuda T, Miyamoto T, Waku K. Distribution of alkyl and alkenyl ether-linked phospholipids and platelet-activating factor-like lipid in various species of invertebrates. *Biochim Biophys Acta*. 1992;1126:298–308.
 74. Brouwers JFHM, Van Hellemond JJ, van Golde LMG, Tielens AGM. Ether lipids and their possible physiological function in adult *Schistosoma mansoni*. *Mol Biochem Parasitol*. 1998;96:49–58.
 75. Chitwood DJ, Krusberg LR. Diacyl, alkylacyl, and alkenylacyl phospholipids of *Meloidogyne javanica* females. *J Nematol*. 1981;13:105–11.
 76. Chitwood DJ, Krusberg LR. Diacyl, alkylacyl and alkenylacyl phospholipids of the nematode *Turbatrix aceti*. *Comp Biochem Physiol B Biochem Mol Biol*. 1981;69:115–20.
 77. Coutant F, Perrin-Cocon L, Agaoglu S, Delair T, Andre P, Lotteau V. Mature dendritic cell generation promoted by lysophosphatidylcholine. *J Immunol*. 2002;169:1688–95.
 78. Rappa G, Mercapide J, Anzanello F, Pope RM, Lorico A. Biochemical and biological characterization of exosomes containing prominin-1/CD133. *Mol Cancer*. 2013;12:62.
 79. van der Kleij D, Latz E, Brouwers JF, Kruize YC, Schmitz M, Kurt-Jones EA, et al. A novel host–parasite lipid cross-talk. Schistosomal lyso-phosphatidylserine activates toll-like receptor 2 and affects immune polarization. *J Biol Chem*. 2002; 277:48122–9.
 80. Spector AA, Yorek MA. Membrane lipid composition and cellular function. *J Lipid Res*. 1985;26:1015–35.